Electronic Supplementary Material (ESI) for Journal of Materials Chemistry A.

Supplementary Information

Computational design of a switchable heterostructure electrocatalyst based on a two-dimensional ferroelectric In_2Se_3 material for the hydrogen evolution reaction

Han Seul Kim*[ab]

[a.] Centre for Supercomputing Applications, National Institute of Supercomputing and Networking, Korea Institute of Science and Technology Information, Daejeon 34141, Republic of Korea

[b.] Department of Data & High Performance Computing Science, University of Science & Technology (UST), Daejeon 34113, Republic of Korea

* hanseulkim0@kisti.re.kr

Supplementary Figures

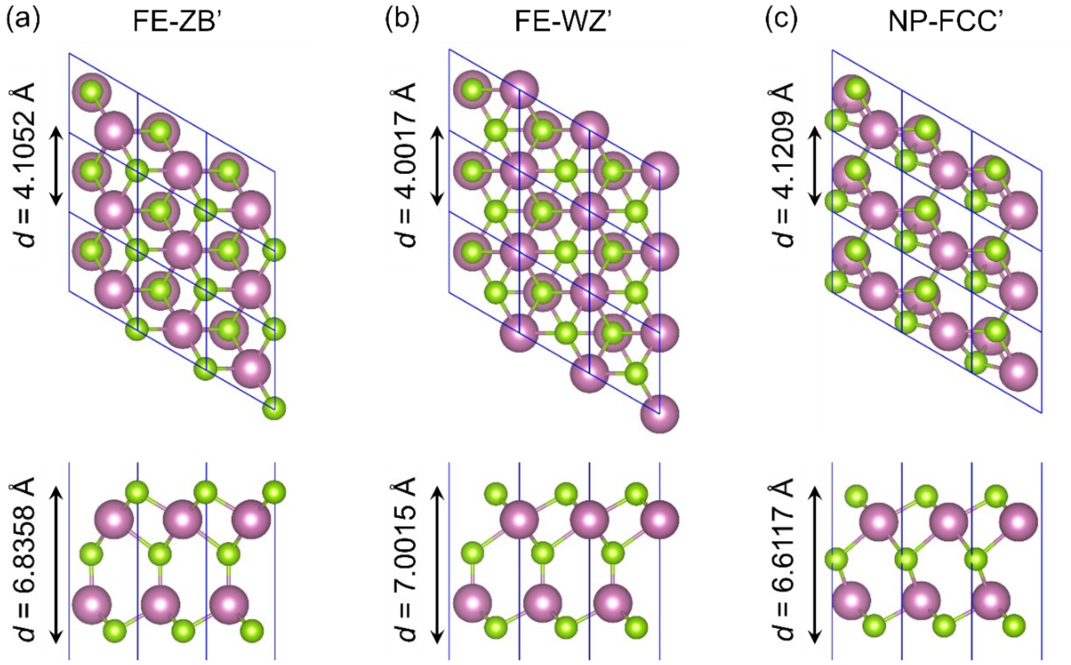

Fig. S1. Three different phases of the quintuple-layer In_2Se_3: (a) ferroelectric zinc blende (FE-ZB'), (b) ferroelectric wurtzite (FE-WZ'), and (c) nonpolar face-centered cubic (NP-FCC') structures. Among the three phases, FE-ZB' and FE-WZ' are two degenerate ground-state structures.

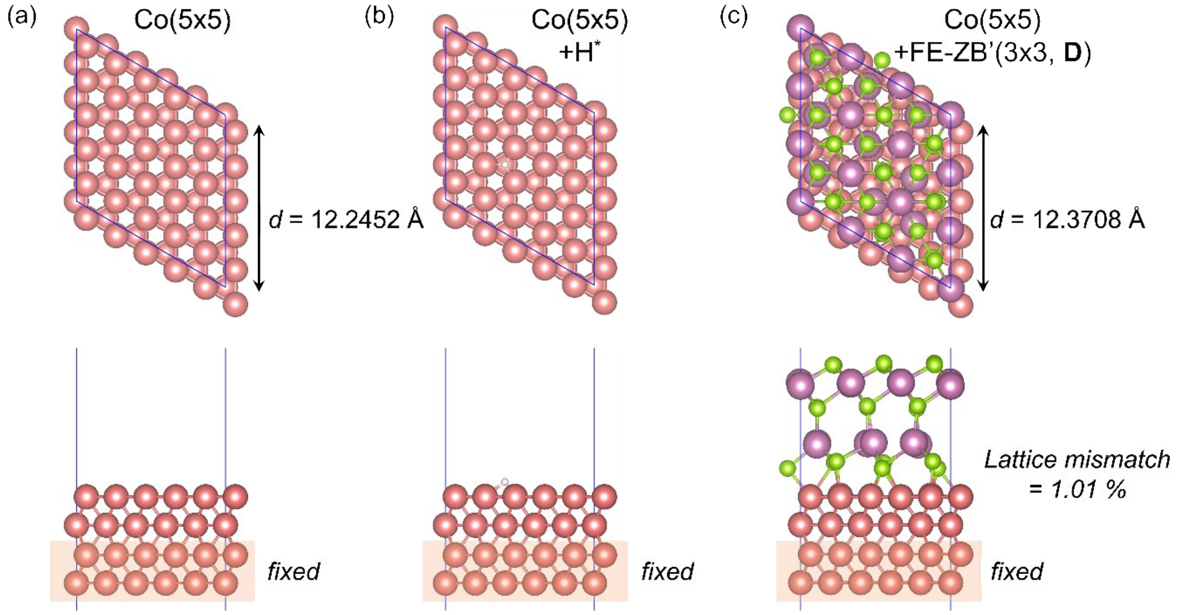

Fig. S2. The top view (top) and side view (bottom) of the atomic models of the catalysts based on cobalt metal substrates: (a) A 5×5 supercell with a four-layer hexagonal close-packed (HCP) cobalt slab (Co (5×5)), (b) Co (5x5) with a hydrogen adsorbent (H^*), and (c) a 3×3 supercell of FE-ZB' with downward polarization (**D**) that is stacked on top of Co (5×5). When obtaining optimized geometries, the atomic positions of the bottom two layers were fixed. The lattice mismatch between Co (5×5) and FE-ZB'(**D**) (3×3) was only 1.01%.

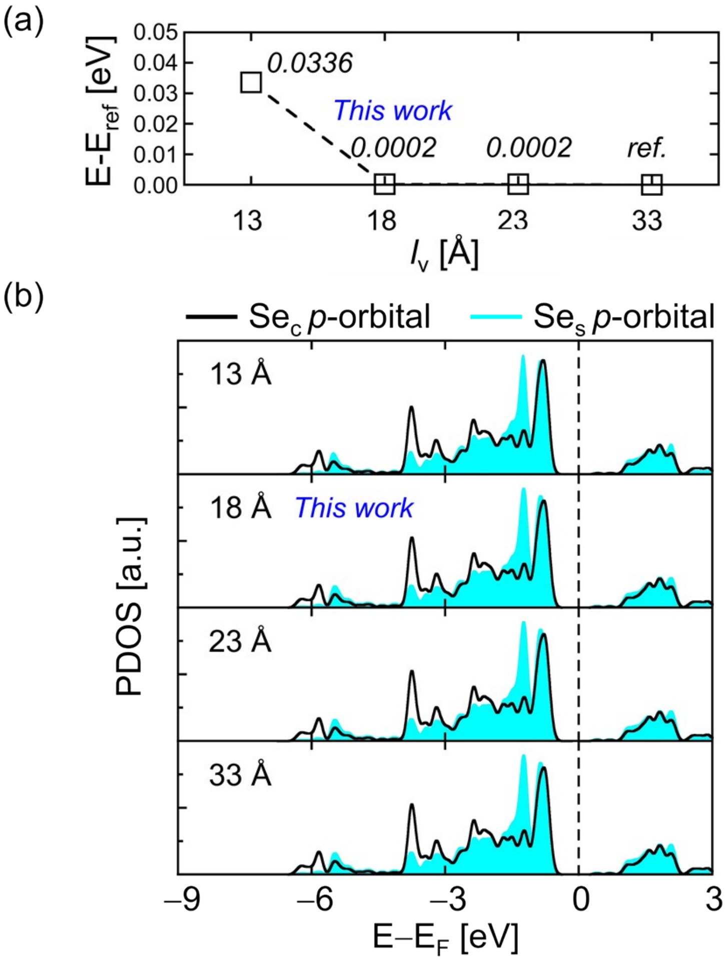

Fig. S3. (a) The relative energy (E_{rel}) as a function of the length of vacuum space (l_v). l_v is the distance between the two neighbouring periodic images along the plane-normal direction of Co+In$_2$Se$_3$ heterostructure, and E_{rel} is defined as $E - E_{ref}$ where E is the total energy and E_{ref} is the total energy of reference system (the case with l_v = 33 Å). The values of E_{rel} for given l_v are written in the plot. (b) Projected density of states (PDOS) with different l_v. The figure confirms that l_v = 18 Å gives the converged energy and PDOS, and this value is adopted in constructing atomic models throughout this study.

k-grid	SCF convergence [eV]	Force convergence [eV]	ΔG_{H^*} [eV]
2 × 2 × 1	10^{-4}	0.05	0.710
2 × 2 × 1	10^{-4}	0.01	0.700
2 × 2 × 1	10^{-5}	0.01	0.701
4 × 4 × 1	10^{-4}	0.05	0.702

Table S1. Values of ΔG_{H*} for In_2Se_3 *1L*(**D**), obtained with different calculation parameters: Monkhorst-Pack *k*-grid, supercell dimensions, and SCF and force convergence criteria. Here, enhancing the self-consistent-field (SCF) convergence criterion for electronic structure calculations and force-convergence criterion for geometry relaxation will change the ΔG_{H*} only by ~0.01 eV.

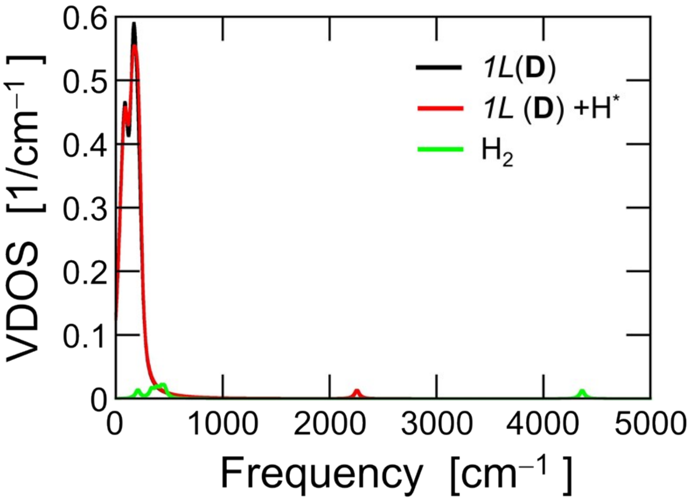

Fig. S4. Vibrational density of states (VDOS) of the species involved in the HER on the monolayer FE-ZB' In_2Se_3 (*1L*) with the downward polarization (**D**) state. Monolayer In_2Se_3 (*1L*(**D**)) with 3×3 supercell, the 3×3 *1L* with an adsorbed hydrogen (*1L*(**D**) + H^*), and the isolated molecular hydrogen (H_2) are indicated by black, red, and green lines, respectively. The values for each case were obtained from the separate calculations without fixing any of the atoms.

Model	**ZPE [eV]**	**ZPE per atom [eV/atom]**	**TS [eV]**	**TS per atom [eV/atom]**
1L(**D**)	1.0275	0.0228	5.0060	0.1112
1L(**D**) + H^*	1.2096	0.0263	5.0088	0.1089
H_2	0.3823	0.1912	0.0775	0.0388

Table S2. The zero-point energies (ZPEs) and entropies multiplied by the temperature (TS) when T = 298.15 K that are obtained for *1L*(**D**), *1L*(**D**) + H^*, and H_2. The values were computed by adopting the VDOS (Fig. S4) which were obtained by using 3×3 supercell *1L*(**D**), 3×3 *1L*(**D**) with an adsorbed hydrogen (*1L*(**D**) + H^*), and the isolated molecular hydrogen (H_2). Focusing on the ZPE divided by the number of atoms, the gas-phase H_2 has higher value than its solid-state counterparts (*1L*(**D**) and *1L*(**D**)+H^*). As can be seen from the Fig. S4, a hydrogen adsorption on *1L* introduces a peak at the high-frequency region (~2200 cm^{-1}); this gives *1L*+H^* a higher ZPE than that of *1L*. However, TS undergoes only a negligible change upon H adsorption because its contribution to low-frequency region is only minute.

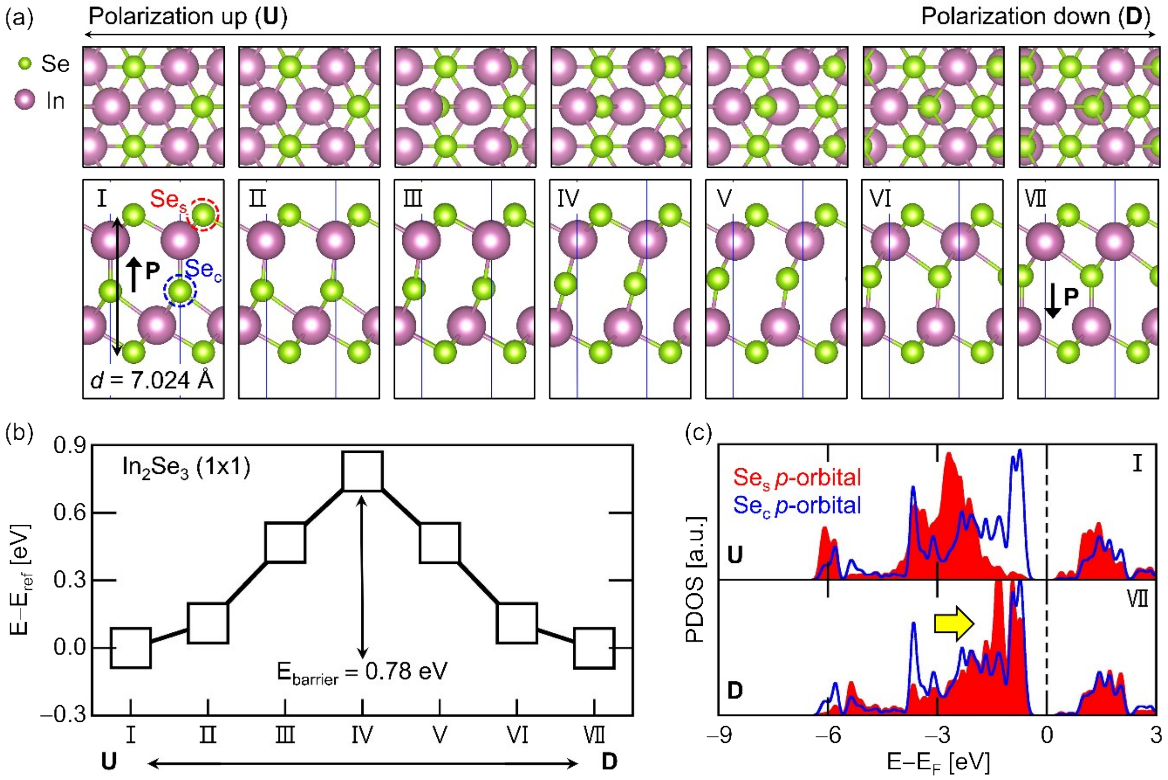

Fig. S5. (a) Atomic models of *1L* FE-ZB' In_2Se_3 with a step-by-step scheme of the polarization switching from **U** to **D**, subdivided from I to VII. The polarization direction and the thickness of *1L* are denoted as **P** and *d*, respectively. Se_s and Se_c indicate the surface and the central Se atoms within *1L*, respectively. (b) The total energies for the unit cell In_2Se_3 of the models from I to VII relative to the total energy of model I (E_{ref}). The calculated energy barrier for the switching is $E_{barrier}$ = 0.78 eV. (c) Projected density of states (PDOS) of the **U** (model I) and **D** (model VII). The *p*-orbital contributions of Se_s and Se_c are indicated by the red shaded area and blue lines, respectively. The yellow arrow indicates the significant upshift of the peak at the valence band contribution of the Se_s *p*-orbital state when switching from **U** to **D**.

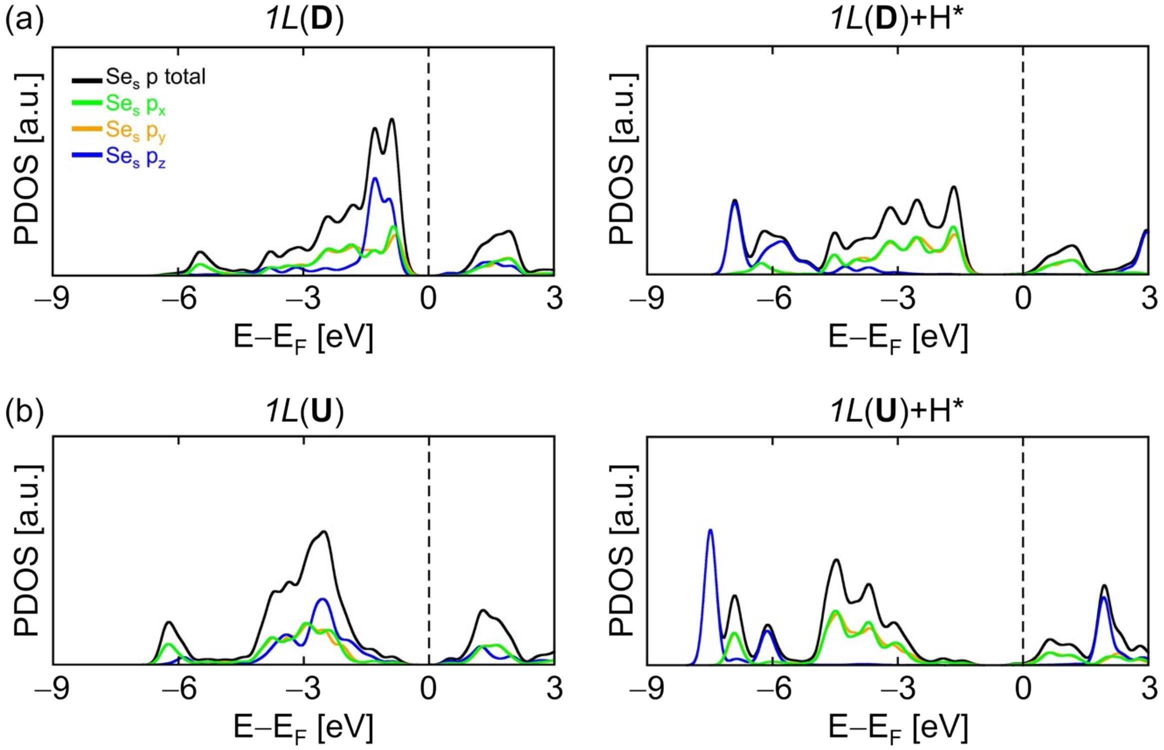

Fig. S6. PDOS for Se$_s$ *p*-orbital contributions for (a) *1L*(**D**) and *1L*(**D**)+H*, and (b) *1L*(**U**) and *1L*(**U**)+H*. Black, green, yellow, and blue lines indicate *p*, p_x, p_y, and p_z orbital contributions of Se$_s$ atoms, respectively. Among others, the p_z orbital contributions below E_F in *1L*(**D**)/*1L*(**U**) greatly move downward after H* adsorptions. This shows that the *p* orbital, specifically the p_z orbital, is the major contributor to the bond formation with H 1s.

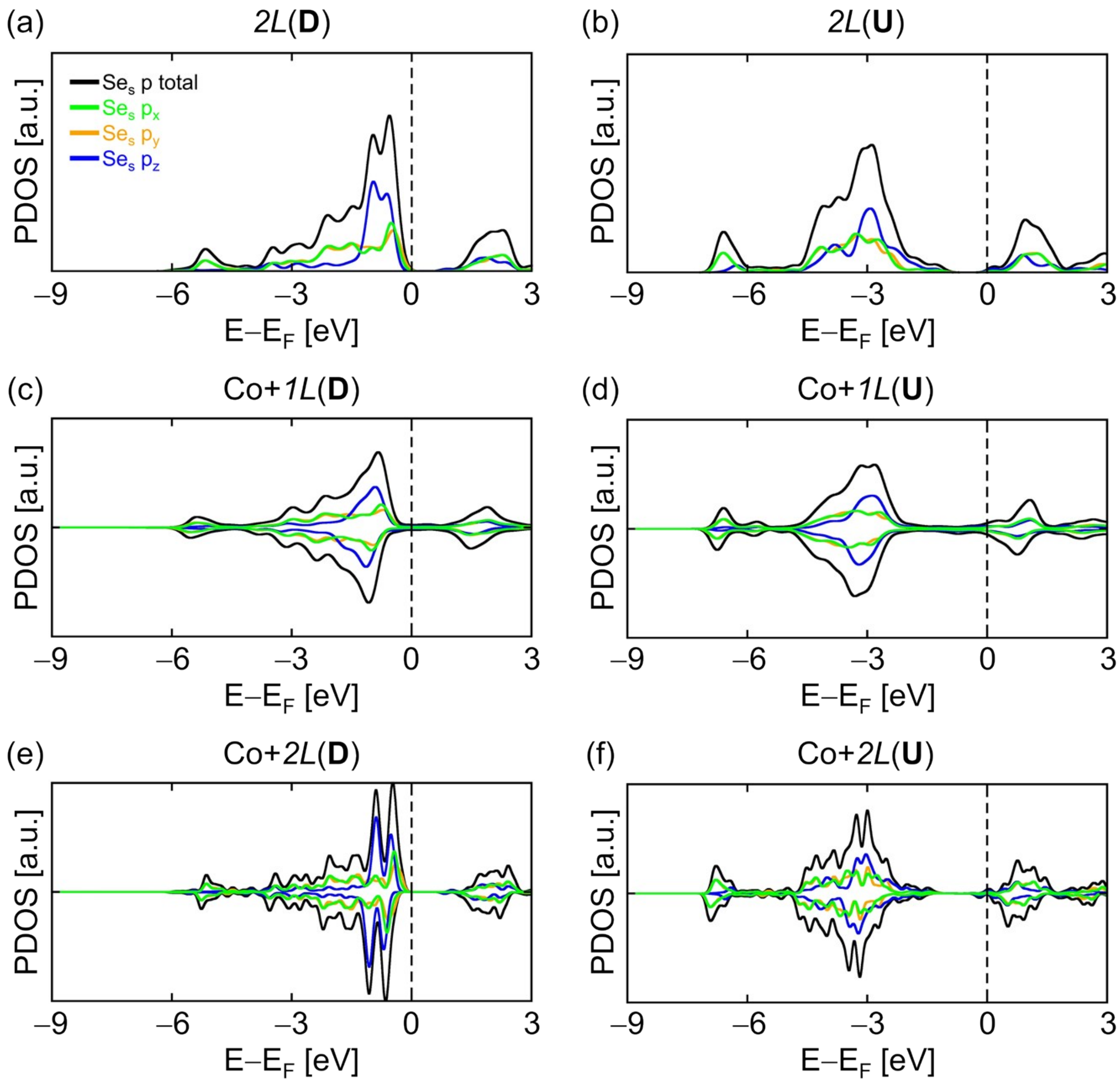

Fig. S7. PDOS for Se$_s$ *p*-orbital contributions for (a) *2L*(**D**), (b) *2L*(**U**), (c) Co+*1L*(**D**), (d) Co+1*L*(**U**), (e) Co+*2L*(**D**), (f) Co+2*L*(**U**). Black, green, yellow, and blue lines indicate *p*, p_x, p_y, and p_z orbital contributions of Se$_s$ atoms, respectively.

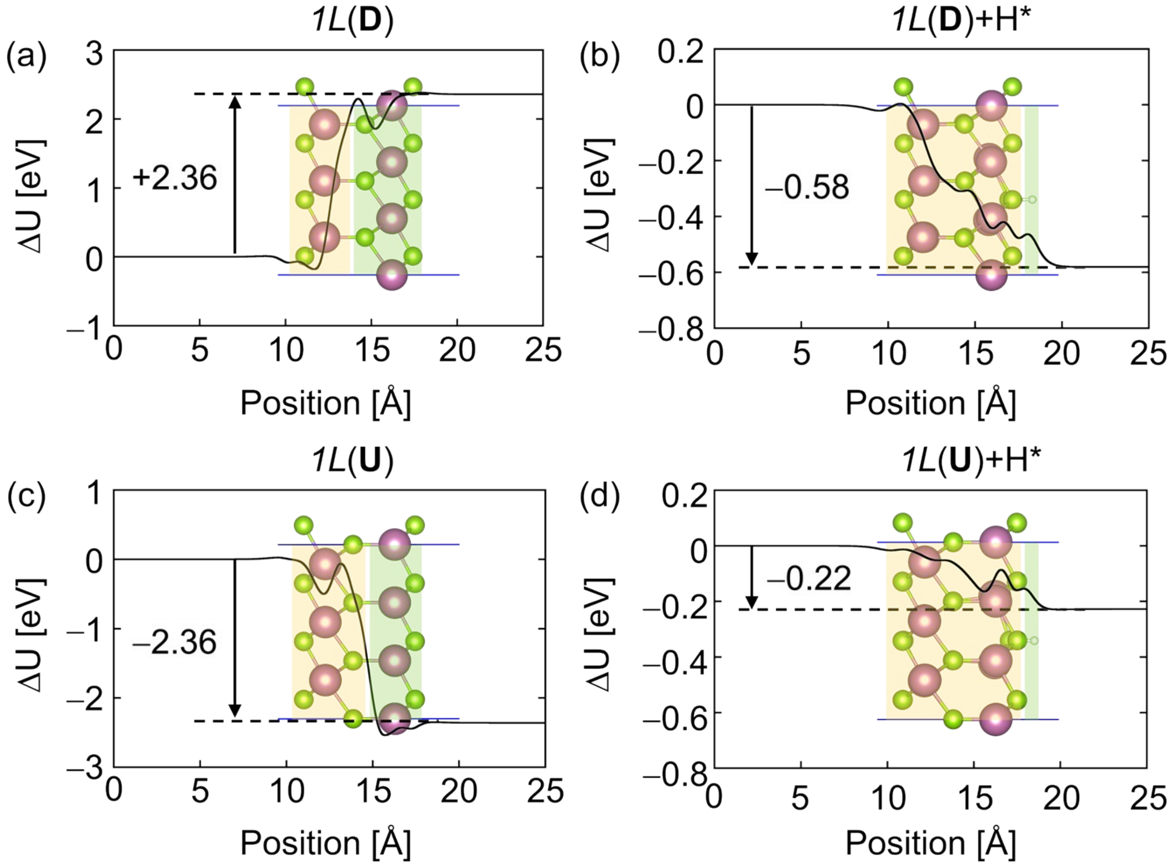

Fig. S8. Change in the potential energy of an electron (ΔU) due to the built-in potential within (a) *1L*(**D**) between InSe and $InSe_2$ sublayers, (b) *1L*(**D**)+H* between *1L*(**D**) and H*, (c) *1L*(**U**) between InSe and $InSe_2$ sublayers, (d) *1L*(**U**)+H* between *1L*(**U**) and H*. Bond dipole (BD) values were obtained as $BD = U_{total} - U_A - U_B$, where U_{total}, U_A, and U_B indicate the potential energies of the system, subsystem A, and subsystem B, respectively. Subsystems A and B are represented by yellow and green shaded areas in each model.[1] BDs for *1L*(**U**) and *1L*(**D**) have the same absolute numbers with opposite signs. Upon hydrogen adsorptions, BDs for *1L*(**D**)+H* and *1L*(**U**)+H* read – 0.58 and – 0.22 eV, respectively. This indirectly implies that the *1L*(**D**) attracts electrons better and forms stronger Se-H bonding with larger BD than *1L*(**U**).

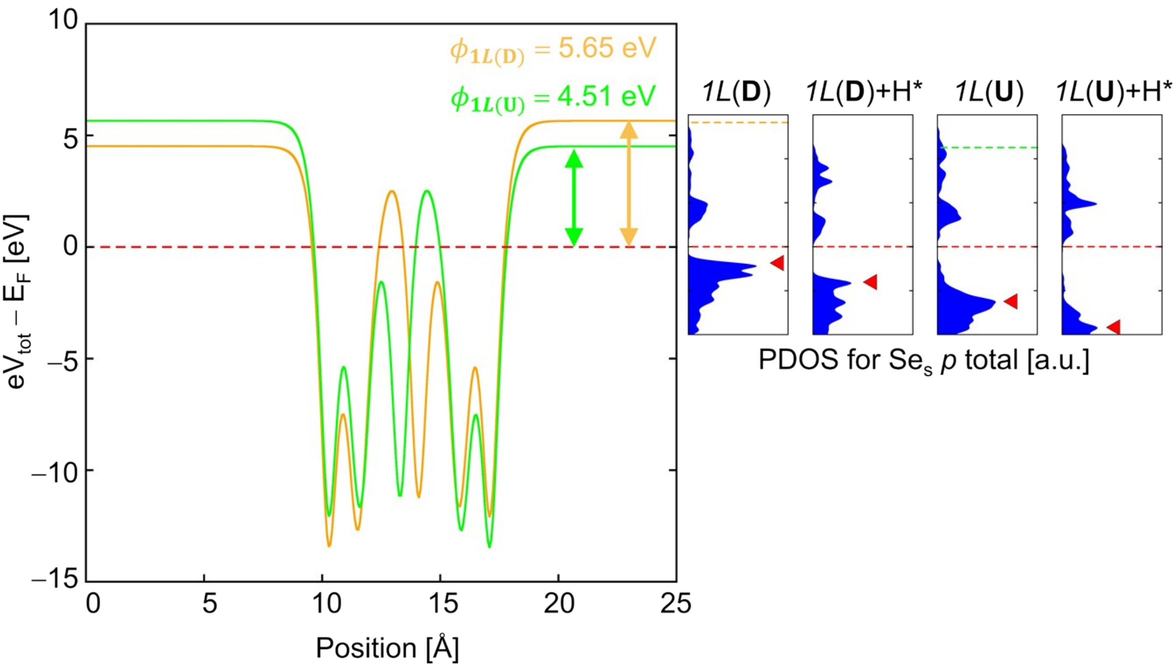

Fig. S9. The potential energies of electron which are aligned with respect to E_F. Yellow and green lines indicate *1L*(**D**) and *1L*(**U**) models, respectively. On the righthand side, a composite PDOS of Se_s *p* orbitals for different models are shown. Red dashed lines indicate E_F. Red downward triangles indicate the location of the first peaks of filled *p*-orbitals. The figure shows that the energy states of *1L*(**D**) locate closer to E_F than those of its *1L*(**U**) counterpart. In both cases, H adsorption further attracts the peaks downwards.

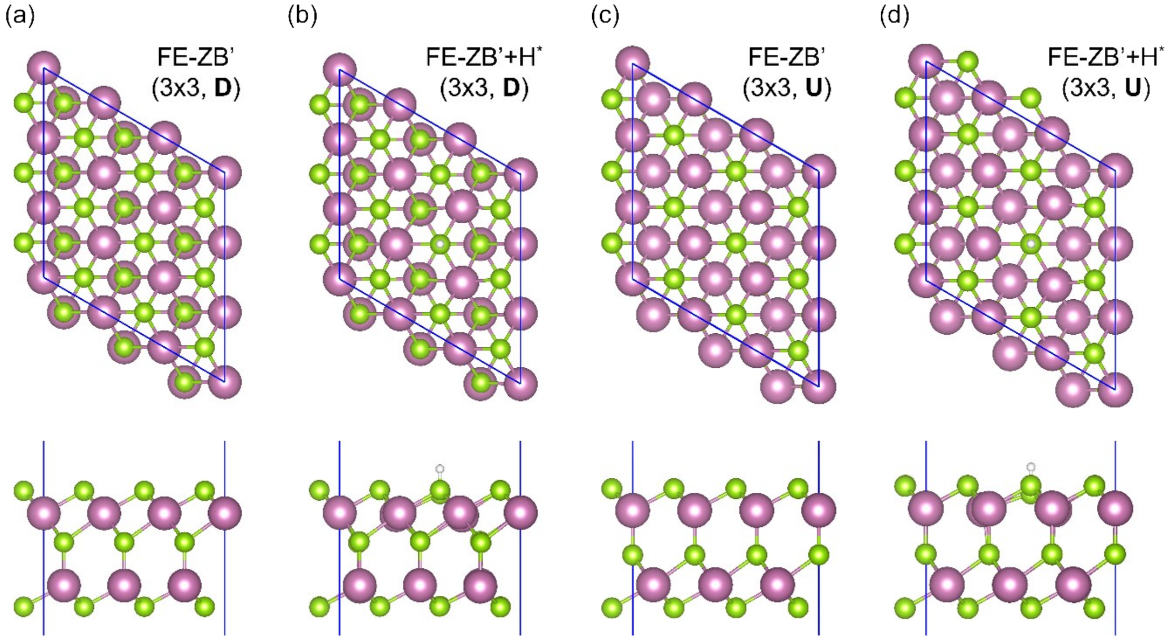

Fig. S10. The atomic structure of the 3×3 supercell (a) FE-ZB′ in the **D** state, (b) FE-ZB′ in the **D** state with H*, (c) FE-ZB′ in the **U** state, and (d) FE-ZB′ in the **U** state with H*.

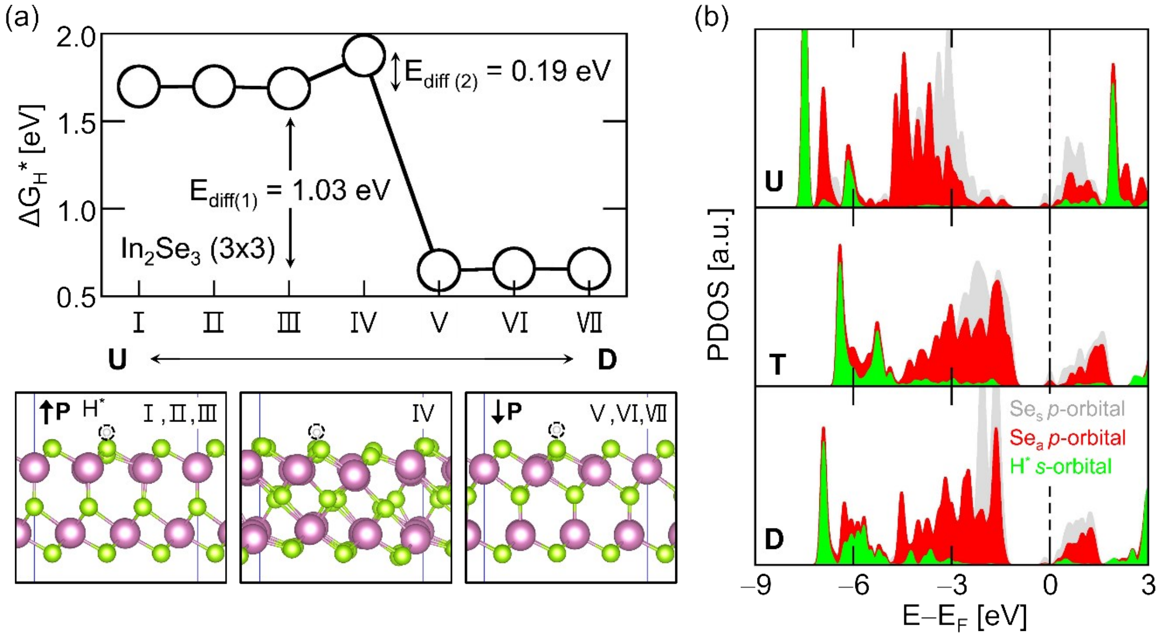

Fig. S11. (a) The free energies of the atomic hydrogen adsorption (ΔG_{H*}) (up) and corresponding atomic structures (down) for the models from I to VII. $E_{diff(1)}$ is defined as the difference in ΔG_{H*} between **U** and **D**, while $E_{diff(2)}$ indicates the ΔG_{H*} difference between **U** and the metastable nonpolar structure (model IV, which is the transition state **T**). (b) PDOS of monolayer In_2Se_3 with **U** (top), **T** (middle), and **D** (bottom) states. Gray, red, and green coloured areas indicate the *p*-orbital of Se_s, the *p*-orbital of Se_a, and the *s*-orbital state of H^*, respectively.

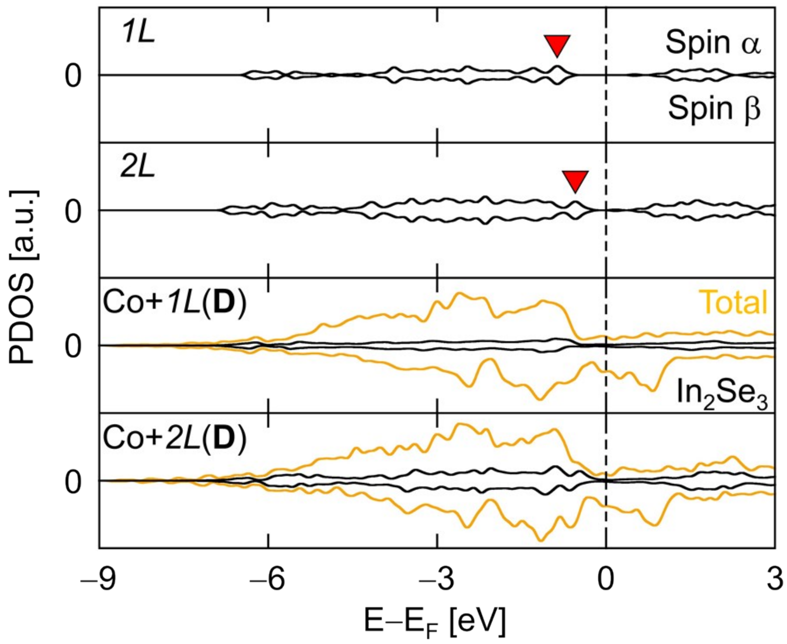

Fig. S12. Spin-resolved PDOS for *1L*, *2L*, Co+*1L*(**D**), and Co+2L(**D**). Black lines indicate PDOS of In_2Se_3 only, while yellow lines represent that of the Co+In_2Se_3 heterostructure. α and β spin components are presented as positive and negative values, respectively. Red downward triangles indicate the $\varepsilon_{\text{p-peak}}$ values for *1L* and *2L*, with values of -0.87 and -0.54 eV, respectively.

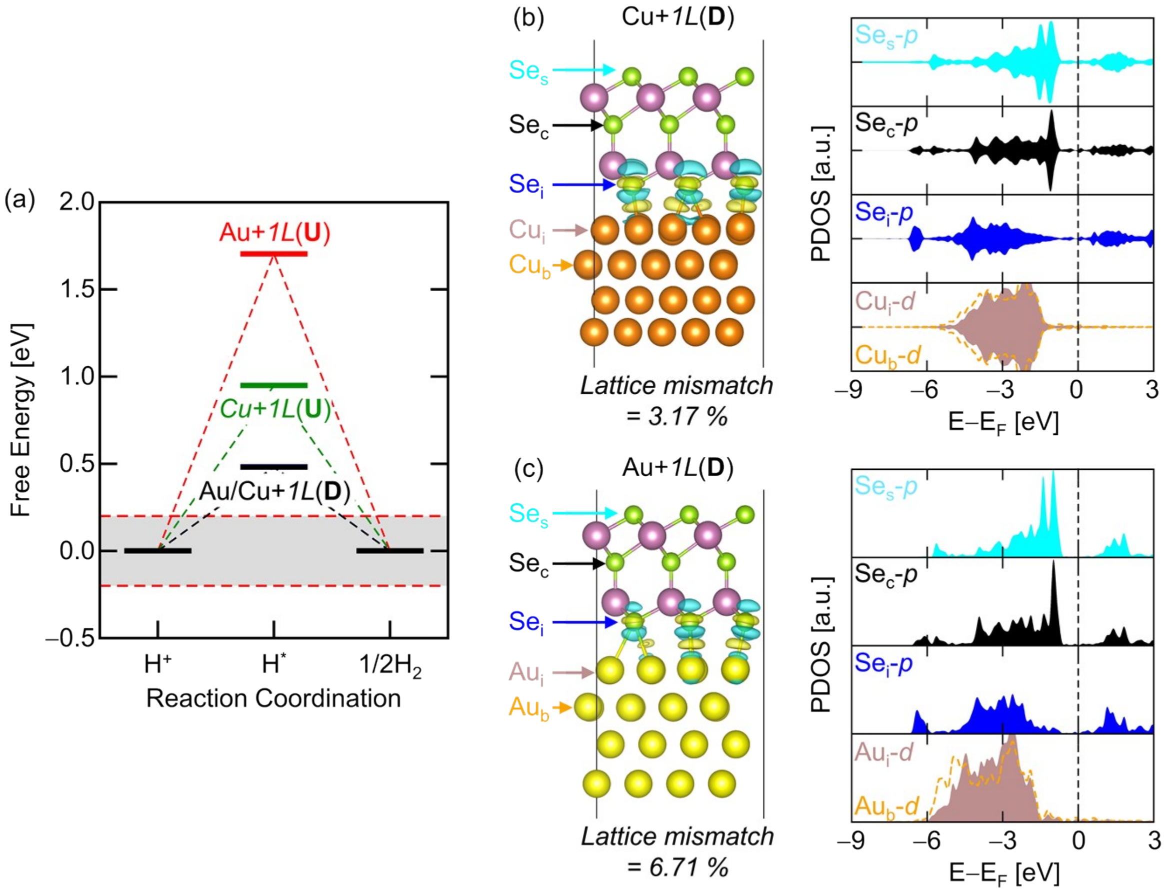

Fig. S13. (a) The free energy diagram for Au/Cu+*1L* cases. The $\varDelta G_{\mathrm{H}*}$ for Au+*1L*(**U**), Cu+*1L*(**U**), and Au/Cu+*1L*(**D**) are 1.702 eV, 0.948 eV, and 0.481 eV, respectively. The values exceed 0.2 eV in all cases, indicating that none of the four cases is favourable for HER. Atomic models that are overlaid with charge density difference (CDD) (left) and spin-resolved PDOS (right) for (b) Cu+*1L*(**D**) and (c) Au+*1L*(**D**). The isovalue is 0.001 **e**/Å^3, while yellow and cyan colours represent positive and negative values, respectively. Cu and Au are reactive and noble diamagnetic metals, respectively, so the α and β spins are degenerated.

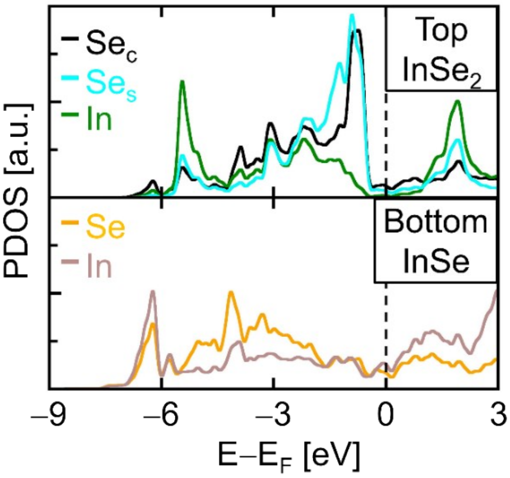

Fig. S14. PDOS of the $InSe_2$ (top) and InSe (bottom) sublayers of the Co+*1L*(**D**) model. The Se atom in the bottom InSe layer is in direct contact with the Co slab, while the Se_s in the top $InSe_2$ layer is exposed as an active surface. The bottom InSe loses its bandgap and becomes metallic, due to the effect of Co slab. Interestingly, even the top $InSe_2$ exhibits finite values in PDOS nearby E_F and shows slight induced metallicity at its bandgap region.

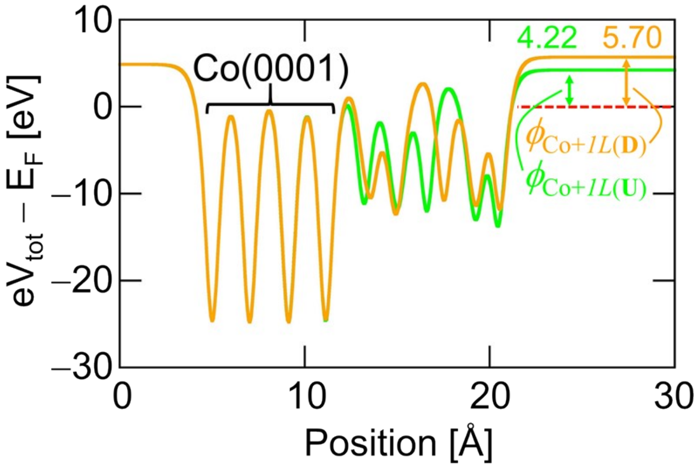

Fig. S15. Plane-averaged total potential energies of Co+*1L*(**D**) and Co+*1L*(**U**) that are indicated by orange and green lines, respectively. The work functions are represented by $\phi_{Co+1L(\mathbf{U})}$ for Co+*1L*(**U**) and $\phi_{Co+1L(\mathbf{D})}$ for Co+*1L*(**D**). $\phi_{Co+1L(\mathbf{U})}$ = 4.22 eV < $\phi_{Co+1L(\mathbf{D})}$ = 5.70 eV indicates that the polarization reversal of the In_2Se_3 effectively modifies the surface potential energies and corresponding surface energy states by ~1.5 eV with the aid of built-in potential.

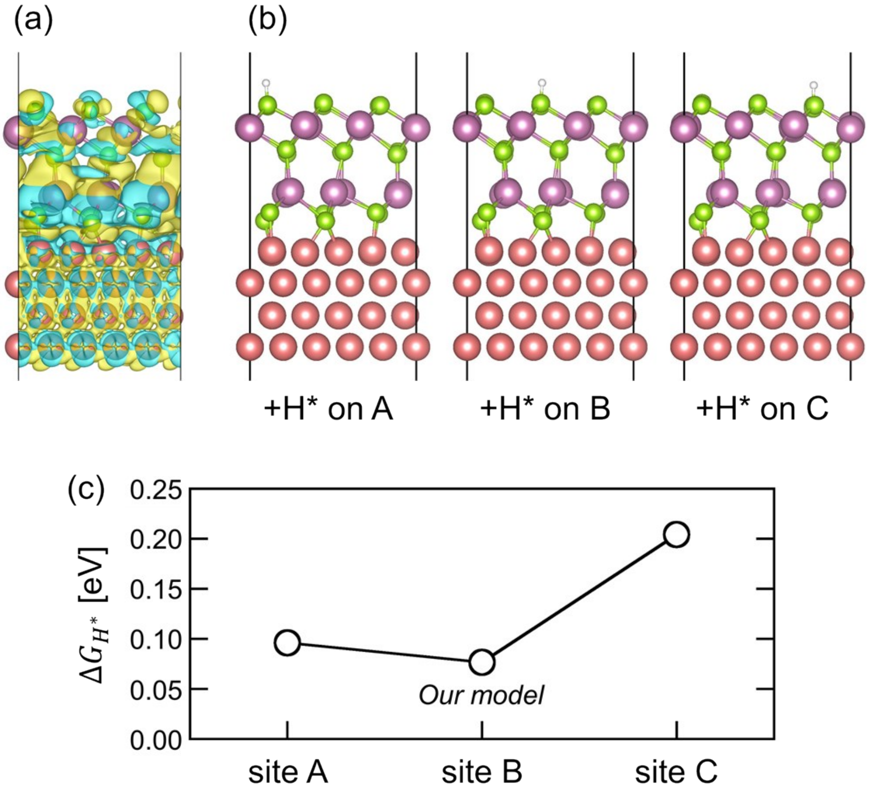

Fig. S16. (a) CDD of Co+1L(D) model, plotted by adopting the isovalue of 0.0002 **e**/Å^3. (b) Atomic models for hydrogen adsorptions on Co+*1L*(**D**) at different adsorption sites; site A, B, and C. (c) ΔG_{H*} obtained for different adsorption sites, and $\Delta G_{H*} < 0.20$ eV for all cases. Site B, which shows the lowest ΔG_{H*}, can be thought of as an active-site Se_s for HER. Electronic structure analysis are shown for the case with site B throughout this paper.

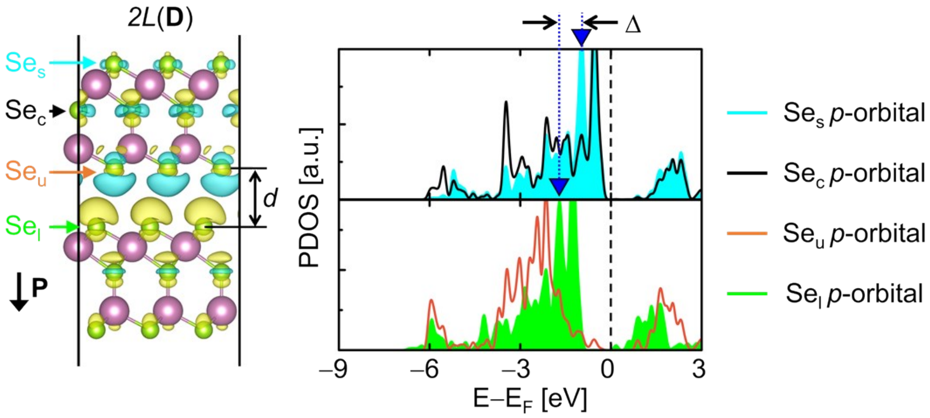

Fig. S17. The charge density difference between the two In_2Se_3 layers (left) and the PDOS (right) for *2L*(**D**). Yellow and cyan colours represent positive (excessive electrons) and negative (deficient electrons) values, respectively. Due to the interface dipole, the upper and the lower layers have noticeable negative and positive CDD values, respectively. The types of atoms in the models are indicated by coloured arrows, and the same colours are used to represent the PDOS: cyan, black, orange, and green represent the *p*-orbitals of Se_s, Se_c, Se_u, and Se_l, respectively. The energy location of the local VBM-1 of outer surface Se atoms of the upper and lower layers (Se_s and Se_l) are marked by the blue downward triangles, and $\Delta = 0.73$ eV quantifies their difference. This indicates that the electron tunnelling channels between the two In_2Se_3 layers through the VBM are unlikely to open for the case with *2L*(**D**). The isovalue is 0.0001 **e**/Å^3, which is only half of the value used in Fig. 3. $d = 3.93$ Å is the interlayer distance between the two layers.

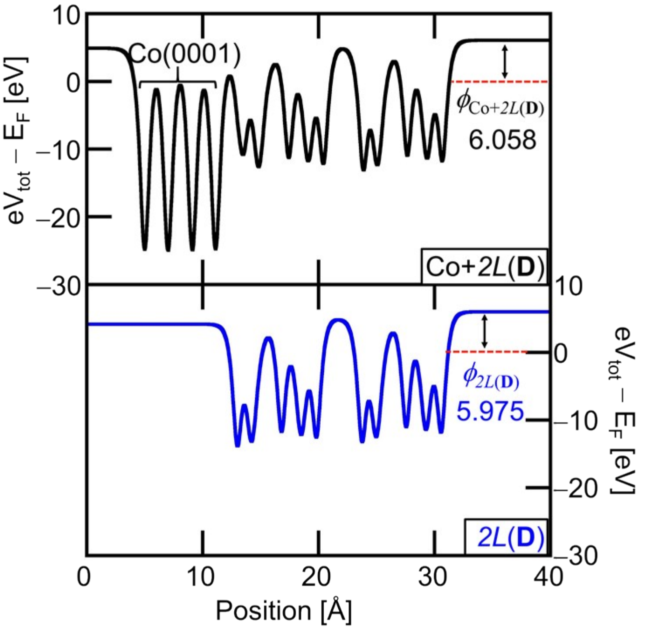

Fig. S18. Plane-averaged total potential energies of Co+*2L*(**D**) (top) and *2L*(**D**) (bottom). The workfunction of the two models differs by ~ 0.1 eV.

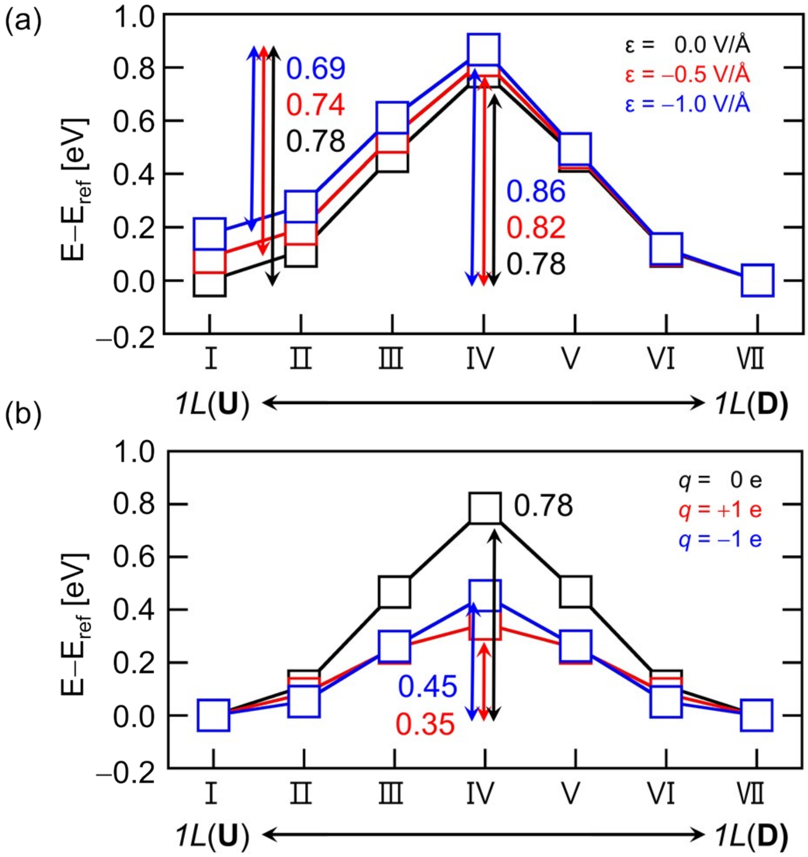

Fig. S19. The modulation of total energies relative to E_{ref} for the free-standing unit cell In_2Se_3 of the models from I to VII (as indicated in Fig. S5), with respect to the (a) applied external electric field ε along the plane-normal direction of In_2Se_3 and (b) net charge q. The reference energy, E_{ref}, refers to the total energy of model VII. Models I and VII respectively indicate *1L*(**U**) and *1L*(**D**). For ε, only the negative values were considered due to the symmetry. The energy barrier for polarization conversion of In_2Se_3 is 0.78 eV per unit cell In_2Se_3 without applying external stimuli. Increasing either ε or q effectively reduces the energy barrier, and further increasing the intensity of these external stimuli will further reduce the energy barrier. This shows that, while the structure of **U** and **D** is stable enough, applying external stimuli will induce the structural conversion between **U** and **D**. The q values were included as non-zero net charge in the simulation cell where the boundary condition for coulomb potential is determined from a multipole expansion, as implemented in GPAW code.[2]

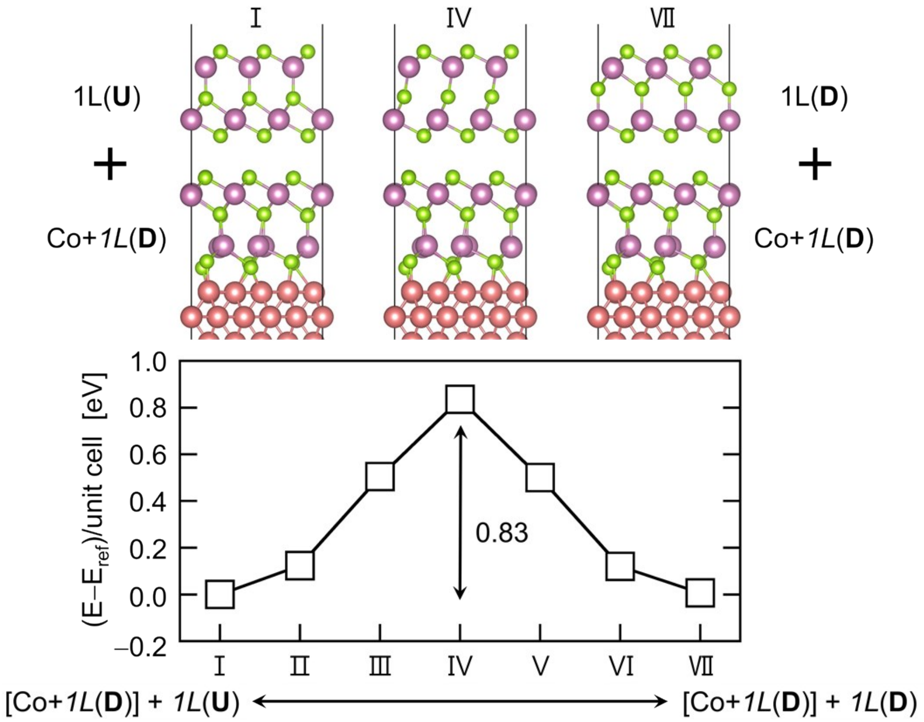

Fig. S20. Total energies relative to E_{ref} Co+*2L* during the polarization switching of the top *1L* from **U** to **D** while the bottom Co+*1L*(**D**) remains unchanged. The reference energy, E_{ref}, refers to the total energy of model VII. The energy barrier for the polarization conversion is obtained as 0.83 eV per unit cell In_2Se_3, so that the increment due to the presence of Co is only 0.05 eV per unit cell.

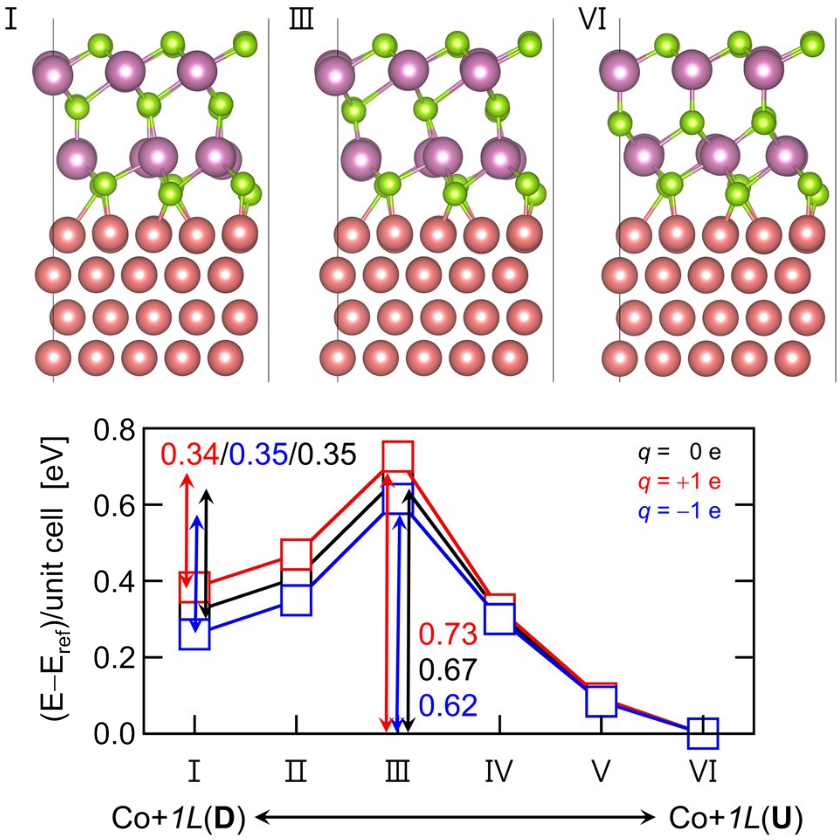

Fig. S21. The modulation of total energies relative to the E_{ref} for the Co+*1L* from I to VI under different net charge q. The reference energy, E_{ref}, refers to the total energy of model VI. The energy is scaled by the unit cell In_2Se_3, and q is for the heterostructure of In_2Se_3 with 3×3 supercell and Co with 5×5 supercell. The energy values in this figure are scaled to the unit cell of In_2Se_3, while the charge q is given for the heterostructure of 3×3 In_2Se_3 and 5×5 Co. Thus, the q = 0, +1, and -1e for this model correspond to the q' = 0, +1/9, and -1/9e for unit cell dimension of In_2Se_3, respectively. The energy barrier per ferroelectric unit is more than 10 times larger than thermal energy (~*kT* where *k* is the Boltzmann's constant and *T* is the temperature), implying its proper stability. Then, applying a negatively larger q will greatly lower the energy barrier. Simultaneously, the energy of Co+*1L*(**D**) relative to Co+*1L*(**U**) will be further reduced. At the end, the energy of Co+*1L*(**D**) can be even lower than that of Co+*1L*(**U**). This indicates that the external stimuli that has a form of backgate bias voltage can induce the polarization conversion between Co+*1L*(**D**) and Co+*1L*(**U**). More thorough theoretical discussions on the ON-OFF conversion dynamics of Co-In_2Se_3 heterostructures within the non-equilibrium external stimuli will be covered in the following study. The q values were included as non-zero net charge in the simulation cell where the boundary condition for coulomb potential is determined from a multipole expansion, as implemented in GPAW code.[2]

Supplementary References

1. G. Heimel, L. Romaner, E. Zojer and J.-l. Bredas, *Acc. Chem. Res.*, 2008, **41**, 721-729.
2. J. Enkovaara, C. Rostgaard, J. J. Mortensen, J. Chen, M. Dułak, L. Ferrighi, J. Gavnholt, C. Glinsvad, V. Haikola, H. A. Hansen, H. H. Kristoffersen, M. Kuisma, A. H. Larsen, L. Lehtovaara, M. Ljungberg, O. Lopez-Acevedo, P. G. Moses, J. Ojanen, T. Olsen, V. Petzold, N. A. Romero, J. Stausholm-Møller, M. Strange, G. A. Tritsaris, M. Vanin, M. Walter, B. Hammer, H. Häkkinen, G. K. H. Madsen, R. M. Nieminen, J. K. Nørskov, M. Puska, T. T. Rantala, J. Schiøtz, K. S. Thygesen and K. W. Jacobsen, *J. Phys. Condens. Matter*, 2010, **22**, 253202.